# Structure of Cytochrome *c*552 from a Moderate Thermophilic Bacterium, *Hydrogenophilus thermoluteolus*: Comparative Study on the Thermostability of Cytochrome *c*‡

Shota Nakamura,[||,#] Shin-ichi Ichiki,[⊥,#] Hiroyuki Takashima,[||] Susumu Uchiyama,[○] Jun Hasegawa,[¶] Yuji Kobayashi,[||,§] Yoshihiro Sambongi,*[,⊥] and Tadayasu Ohkubo*[,||]

*Graduate School of Pharmaceutical Sciences, Osaka University, Suita, Osaka 565-0871, Japan, Graduate School of Biosphere Science, Hiroshima University, Higashi-Hiroshima, Hiroshima 739-8528, Japan, Graduate School of Engineering, Osaka University, Suita, Osaka 565-0871, Japan, Daiichi Pharmaceutical Co., Ltd., Edogawa-ku, Tokyo 134-8630, Japan, and Osaka University of Pharmaceutical Sciences, Takatsuki, Osaka 569-1094, Japan*

*Received October 4, 2005; Revised Manuscript Received February 22, 2006*

ABSTRACT: We have studied the structure−thermostability relationship using cytochromes *c* from mesophilic and thermophilic bacteria; *Pseudomonas aeruginosa* (PA$c_{551}$) growing at 37 °C and *Hydrogenobacter thermophilus* (HT$c_{552}$) at 72 °C and showed that only five residues primarily differentiate their stabilities. For a more comprehensive study, we found *Hydrogenophilus thermoluteolus* (*Pseudomonas hydrogenothermophila*) growing at 52 °C and showed the moderate stability of the cytochrome *c* from this bacterium (PH$c_{552}$). To explore the stabilization mechanisms, the crystal structure of PH$c_{552}$ was determined by X-ray analysis. The solution structure of HT$c_{552}$ elucidated previously by NMR was refined using distributed computational implementation. Furthermore, the recently reported crystal structure of HT$c_{552}$ has become available [Travaglini-Allocatelli, C. et al. (2005) *J. Biol. Chem. 280*, 25729−25734]. When the structures of these three cytochromes *c* were combined, this revealed that the five residues, corresponding to those mentioned above, determine the difference of stabilities among them as well. These facts suggested the stabilization mechanisms as follows: (1) improved van der Waals interactions by packing optimization at the N-terminal helix, (2) attractive electrostatic interactions with the heme propionate group, and (3) favorable van der Waals interaction with the heme. This comparative study, by supplementing the structural information of PH$c_{552}$ with its complementary feature, demonstrates that just a small number of amino acid residues determine the overall molecular stability by means of additivity of the effects of their substitutions. It is interesting that, in naturally occurring proteins, these adaptation strategies are accommodated by these bacteria to survive in the wide range of thermal conditions.

Bacterial microorganisms are distributed in a wide range of thermal conditions from subfreezing to over boiling temperatures. It has been well-known that the thermal stabilities of proteins are related to their growth temperature; for example, the denaturation temperature of the proteins from thermophilic bacteria are usually higher than that of mesophilic bacteria (*1*, *2*). The mechanism which provides these various stabilities using the limited number of amino acids attracts our attentions. Various comparative studies on this problem have been carried out at the genomic and protein levels. For example, a comparison of amino acid composition of proteins produced by mesophilic and thermophilic bacteria revealed a 2-fold decrease in the frequency of glutamine and an increase of tyrosine among thermophiles (*3*). However, such differences of composition of total proteins among different bacteria are too vague to provide any clue about the stabilizing mechanisms. A comparison of the relationship between amino acid sequence and structure of a specific protein produced by a thermophilic bacterium with that of its counterpart homologous protein produced by a mesophilic bacterium should simplify the situation to disclose the basis of stability. Although the overall structures of homologous proteins often look so similar that it had been rather difficult to find distinct differences among them, the development of structural biology supported by gene technology has made it possible to make such analyses through detailed structures. Various protein structures were investigated from the aspect of evolution, such as dehydrogenase (*4*) and rhodanese (*5*).

‡ The atomic coordinates and structure factors (PDB codes: 2D0S for crystal structure of cytochrome *c*552 from *Hydrogenophilus thermoluteolus* (PH$c_{552}$) and 2AI5 for solution structure of cytochrome *c*552 from *Hydrogenobacter thermophilus* (HT$c_{552}$)) have been deposited in the Protein Data Bank, Research Collaboratory for Structural Bioinformatics, Rutgers University, New Brunswick, NJ (http://www.rcsb.org/).

* Corresponding authors. Yoshihiro Sambongi, Graduate School of Biosphere Science, Hiroshima University, 1-4-4 Kagamiyama, Higashi-Hiroshima, Hiroshima, 739-8528, Japan; tel and fax, +81 82 424 7924; e-mail, sambongi@hiroshima-u.ac.jp. Tadayasu Ohkubo, Graduate School of Pharmaceutical Sciences, Osaka University, 1-6 Yamadaoka, Suita, Osaka 565-0871, Japan; tel, +81 6 6879 8223; fax, +81 6 6879 8221; e-mail, ohkubo@protein.osaka-u.ac.jp.

|| Graduate School of Pharmaceutical Sciences, Osaka University.

⊥ Graduate School of Biosphere Science, Hiroshima University.

# These authors contributed equally to this work.

○ Graduate School of Engineering, Osaka University.

¶ Daiichi Pharmaceutical Co., Ltd.

§ Osaka University of Pharmaceutical Sciences.

10.1021/bi0520131 CCC: $33.50 
Published on Web 04/20/2006

Studies on cytochrome *c* (*6*), ribonuclease $H_1$ (*7*), and methanococcal adenylate kinase (*8*−*10*) are examples of comparative analyses.

Since we determined a structure of cytochrome *c* from a thermophilic bacterium by NMR[1] (*11*), we have also performed such a series of comparative studies on this protein (*6*). Cytochrome *c*, which plays a main role in the electron-transfer reaction, is a ubiquitous protein distributed over a wide range of species from prokaryotes to eukaryotes. Thus, cytochrome *c* proteins available from various organisms living under diverse environmental conditions, such as extremely low or high temperatures, are suitable targets for our investigation.

In the previous work, we have reported the comparative studies on a pair of proteins, that is, cytochrome *c*551 from *Pseudomonas aeruginosa* (PA$c_{551}$) growing at 37 °C, a model of mesophilic protein, and cytochrome *c*552 from *Hydrogenobacter thermophilus* (HT$c_{552}$) growing at 72 °C, a model of thermophilic protein (*12*). These proteins showed quite different thermal stabilities, such that the unfolding temperatures were 86.4 °C for PA$c_{551}$ and 121.1 °C for HT$c_{552}$ (*13*). It is noteworthy that, even though these two proteins show 56% sequence identity, HT$c_{552}$ is highly tolerant of high temperature. Careful comparison of the two structures and the site-directed mutagenesis on PA$c_{551}$ enabled us to identify five residues which contribute predominately to the difference of the thermal stabilities of these proteins. Actually, when these five residues of PA$c_{551}$ were substituted by the corresponding five residues of HT$c_{552}$, PA$c_{551}$ had an enhanced stability close to that of HT$c_{552}$ (*14*). Meanwhile, the reciprocal substitution of the five residues from HT$c_{552}$ to PA$c_{551}$ resulted in the decreased thermal stability of HT$c_{552}$ close to that of PA$c_{551}$ (*13*). These swapping experiments also revealed that each of these five residues affects stability independently and that they contribute to the overall stability of the protein in an additive manner (*15*).

In this work, we selected cytochrome *c*552 (PH$c_{552}$) from a moderate thermophilic bacterium, *Hydrogenophilus thermoluteolus* (formerly named as *Pseudomonas hydrogenothermophila*), that grows at 52 °C to carry out a more comprehensive study on the structure and stability relationship. This PH$c_{552}$ shares sequence identities of 50.6% with PA$c_{551}$ and 54.4% with HT$c_{552}$, and has a moderate stability.

A set of three cytochromes *c* with relatively high, middle, and low stabilities enabled us to investigate further how the difference of structures reflects on their stabilities. However, the structural difference among them is likely not large because even PA$c_{551}$ and HT$c_{552}$ resemble each other overall. To obtain more precise structural information, we crystallized PH$c_{552}$ as reported preliminarily (*16*). Here, the results of the X-ray analysis of this crystal of PH$c_{552}$ will be discussed first.

Very recently, the crystal structure for HT$c_{552}$ was reported by Travaglini-Allocatelli et al. (*17*). This made it possible to compare the crystal structures of three cytochromes *c*. However, for the crystal structure of HT$c_{552}$, there was the possibility that the crystallization reagents affected the orientation of the side chains of interest. Thus, using distributed computational calculations (*18*−*20*), we highly refined its solution structure, which we had determined with NMR, and estimated the effects of the reagents.

Using these detailed structures, we challenged ourselves to test and prove that our previous hypothesis is correct. We reasoned that if the information obtained previously from the two proteins was correct, that is, cytorhcome *c* stability is determined by a proper combination of just five residues, then it should explain the stability of another naturally occurring protein, that is, one from a moderate thermophilic bacterium.

The results below confirm our assumption. This unique test begins to provide some rudimentary principle of protein structure and stability. Understanding protein stability is the necessary basis for strategies to design thermostable enzymes of bioindustrial interest.

## MATERIALS AND METHODS

*Protein Preparation.* The overexpression of PH$c_{552}$ and the correct post-translational modification in *Escherichia coli* have been achieved by the method which was previously used in the case of HT$c_{552}$ where the signal sequence was changed to that of PA$c_{551}$ and the cytochrome *c* maturation (*ccm*) genes were coexpressed (*13*, *21*). PH$c_{552}$ was overexpressed with co-transformed pEC86 carrying *ccm* genes in *E. coli* JCB387 cells and purified from the periplasmic protein fractions as previously described (*16*). Initially, PH$c_{552}$ was purified by Hi-Trap Q column chromatography at pH 8.0, and further purification was carried out by Hi-Trap SP column chromatography (Amersham Biosciences) with a sodium chloride concentration gradient (0−500 mM) in 25 mM sodium acetate buffer at pH 5.0. Finally, gel-filtration chromatography was performed with a Superdex 75 column equilibrated and eluted with 25 mM sodium acetate buffer at pH 5.0. The eluted solution of PH$c_{552}$ was concentrated to 40 mg/mL by ultrafiltration (Centriplus YM-3, Millipore) and sterile-filtered (0.1 $\mu$m Ultrafree-MC, Millipore). It was confirmed that the heterologously expressed PH$c_{552}$ exhibited the same spectroscopic and electrochemical properties as those of the authentic protein (*16*).

*Thermal Unfolding.* The complete thermal-unfolding profile of PH$c_{552}$ was acquired using a recently developed pressure-proof cell compartment installed in the CD spectrometer which enables us to obtain spectra over 100 °C by keeping the solution under 10 atm (*22*). It has been shown that thermal-unfolding profiles in the pressure-proof cell compartment at 10 atm are the same as those in the ordinary cell compartment at 1 atm (*23*). CD measurements were carried out under oxidative conditions where no absorption was detected from reduced cytochrome *c* in UV−visible spectra. The temperature dependence of the CD ellipticity at 222 nm was monitored at every 5 °C from 60 to 140 °C using a 1 mm path length cuvette in a JASCO J-720 spectrophotometer. The samples with protein concentrations of 10 $\mu$g/mL were adjusted with HCl to pH 5.0. The CD ellipticity around the unfolding midpoint was measured at 2 °C intervals with a thermal equilibrium time of 2 min.

[1] Abbreviations: PA$c_{551}$, cytochrome $c_{551}$ from *Pseudomonas aeruginosa*; PH$c_{552}$, cytochrome *c*552 from *Hydrogenophilus thermoluteolus* (*Pseudomonas hydrogenothermophila*); HT$c_{552}$, cytochrome *c*552 from *Hydrogenobacter thermophilus*; CD, circular dichroism; Gdn-HCl, guanidine hydrochloride; NMR, nuclear magnetic resonance; MPD, 2-methyl-2,4-pentandiol; rmsd, root-mean-square deviation; $T_m$, the temperature at the midpoint of transition; $C_m$, the concentration of Gdn-HCl at the midpoint of transition.

Thermodynamic parameters based on the two-state unfolding profiles were obtained using nonlinear least-squares fitting with MATHEMATICA ver.5.0 employing the van't Hoff equation and the Gibbs−Helmholtz equation as described previously (*23*, *24*). The thermodynamic parameters were determined by averaging those obtained by more than three different independent measurements. To show that the unfolding of PH$c_{552}$ was highly reversible, after the completion of the heating process up to 110 °C, the sample was cooled and kept at 40 °C. From the spectra at 40 °C, before and after heating, it was confirmed that 98% of the native structure was recovered (Supporting Informatiion, Figure 1).

*Guanidine Hydrochloride Denaturation.* Stability of PH$c_{552}$ against chemical denaturants was assessed by guanidine hydrochloride (Gdn-HCl)-induced denaturation experiments. The CD ellipticity at 222 nm was monitored using a 1 mm path length cuvette at 25 °C. To equilibrate the proteins with the denaturant, proteins of 10 $\mu$g/mL were incubated in various concentrations (0.0−6.0 M) of Gdn-HCl solutions, which were adjusted with HCl to pH 5.0, at 25 °C for 2 h before measurements. The observed data were fitted by linear least-squares fitting with MATHEMATICA ver.5.0 employing the Marquart−Levenberg algorithm using a linear extrapolation model (*25*).

*Crystallization and Data Collection*. All crystallization experiments were performed by the hanging drop vapor diffusion method. Small plate-shaped crystals of PH$c_{552}$ were obtained at 4 °C with 30% (w/v) poly(ethylene glycol) 4000 and 0.1 M Mes (pH 6.5). Preliminary X-ray studies were already reported (*16*). The diffraction data were collected from the crystal grown under the same conditions to generate a well-defined diffraction pattern, on a RIGAKU R-axis IV$^{++}$ imaging plate detector equipped with a MicroMax007 rotating anode generator running at 40 kV and 20 mA, using Cu K$\alpha$ radiation. X-ray intensity data were indexed, integrated, and subsequently scaled using Crystal Clear ver.1.3.5 software (*26*). The crystals, which diffract to a resolution limit of 2.2 Å, belong to the orthorhombic space group $C222_1$, with unit cell parameters of $a = 49.25$, $b = 58.41$, $c = 56.32$ Å. A molecular replacement solution for PH$c_{552}$ was found using MOLREP (*27*) with the molecular model of PA$c_{551}$ (PDB code: 351C). The data statistics are shown in Table 1.

*Model Building and Refinement.* The model obtained from molecular replacement method was subjected to the rigid body refinement in the program CNS (*28*), providing the *R*-factor of 28.3%. Then, the model building followed by CNS refinements with water picking, simulated annealing, and minimization was carried out over several rounds until the *R*-factor was equal to 20%. The final stage of refinement was conducted with the program REFMAC5 (*29*), and the resulting model was refined manually by using the program XtalView (*30*). The *R*-factor of the final model was 18.1% ($R_{free}$ 21.8%). Detailed refinement statistics are summarized in Table 1. The structure quality was evaluated using PROCHECK (*31*). Secondary structure characterizations were carried out using the program DSSP (*32*). A refined model was deposited in PDB (PDB code: 2D0S). Multiple sequence alignment and pairwise least-squares fit were performed by using PROFIT (*33*). The drawings of molecular figures were generated using PyMOL (*34*) for crystal structures and MOLMOL (*35*) for solution structures.

Table 1: Data Collection and Refinement Statistics

| data collection | home source |
|---|---|
| temperature (K) | 293 |
| space group | $C222_1$ |
| cell dimensions *a*, *b*, *c* (Å) | 49.25, 58.41, 56.32 |
| resolution limits (Å) | 50.00−2.20 (2.28−2.20)[a] |
| no. unique/observed reflections | 4086/17886 |
| average redundancy | 4.40 (3.9) |
| completeness (%) | 94.4 (75.3) |
| $R_{merge}$[b] (%) | 8.0 (18.4) |
| **refinement statistics** | |
| refinements resolution range (Å) | 9.74−2.20 |
| $R/R_{free}$[c] (%) | 18.1/21.8 |
| rmsd from ideal | |
| bonds (Å) | 0.023 |
| angles (deg) | 1.434 |
| $\langle B \rangle$ for atomic model[d] (Å$^2$) | 20.47 |
| Ramachandran plot | |
| most favored regions (%) | 92.2 |
| additional allowed regions (%) | 6.2 |
| generously allowed regions (%) | 1.6 |
| disallowed regions (%) | 0.0 |

[a] Values in parentheses indicate the data in the highest resolution shell. [b] $R_{merge} = \sum|I_h - \langle I_h \rangle|/\sum I_h$, where $\langle I_h \rangle$ is the average intensity of reflection h and symmetry-related reflections. [c] $R$ and $R_{free} = \sum||F_o| - |F_c||/\sum|F_o|$ calculated for reflections of the working set and test (10%) set, respectively. [d] $\langle B \rangle$ is the average temperature factor for all protein atoms.

*Refinements of HT$c_{552}$ Solution Structure by Using Distributed Computational Implementation.* The NMR experimental data deposited in PDB (PDB code: 1AYG) were subjected to the structure refinement using distributed computational implementations (*18*−*20*). The restraint molecular dynamics calculations used XPLOR-NIH ver. 2.0.6 (*36*) on the distributed computing of 20 Linux PCs controlled by SUN GRID engine ver. 5.3 p2. In the previous papers (*18*−*20*), we demonstrated that the overall convergence of the resulting structures obtained from NMR and distance geometry calculations is based not only on the quality of experimental data but also on the extent of the explored conformational space. When we start the structure calculation by generating thousands of initial structures, it is possible to search a wide conformational space avoiding those trapped in localized folds. The calculations were started by generating initial structures from a random array and were followed by 500 ps simulated annealing (SA) at a high initial temperature, 5000 K. The total number of initial structures was 4000, and 20 final structures with the lowest energies of target function were selected as a solution structure ensemble which was deposited in PDB (PDB code:2AI5).

## RESULTS AND DISCUSSION

*Thermal and Chemical Stability of PH$c_{552}$.* Thermal and chemical denaturation curves of PA$c_{551}$, PH$c_{552}$, and HT$c_{552}$ are shown in Figure 1. These denaturation experiments were performed under the same conditions: the same pH 5.0 and the same protein concentration of 10 $\mu$g/mL. The denaturation curves gave S-shaped curves that resembled a two-state unfolding transition. Table 2 provides the thermodynamic parameters for the thermal denaturation obtained by van't Hoff and Gibbs−Helmholtz equations with the nonlinear fitting procedure. In the thermal denaturation experiment, the $T_m$ value for PH$c_{552}$ was found to be 108.0 °C,

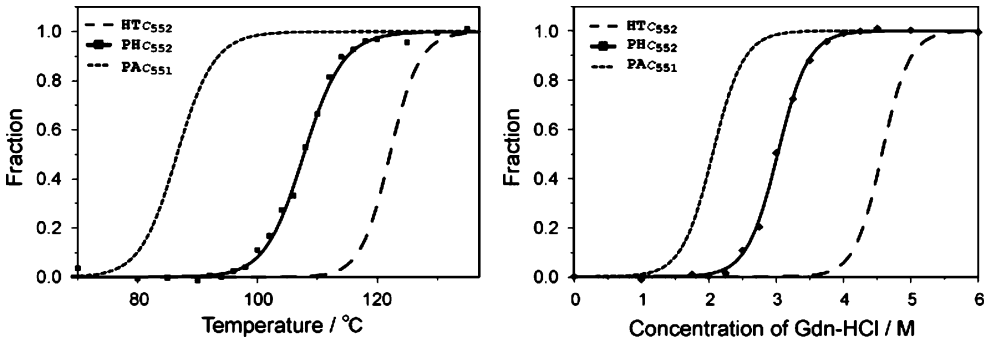


FIGURE 1: Thermal and chemical denaturation curves. The unfolded fractions are plotted as a function of temperature (left panel) and concentration of Gdn-HCl (right panel). The denaturation curves of PA$c_{551}$, PH$c_{552}$, and HT$c_{552}$ are represented by a short-dashed line, solid line, and dashed line, respectively. The black circles represent the observation points. The curves of PA$c_{551}$ and HT$c_{552}$ are redrawn based on the previous results (*13*).

Table 2: Thermodynamic Parameters Obtained from Thermal Denaturation

| | $\Delta H(T_m)$ (kcal mol$^{-1}$) | $\Delta S(T_m)$ (kcal mol$^{-1}$ K$^{-1}$) | $T_m$ (°C) | $\Delta G(T_m, PHc_{552})$ (kcal mol$^{-1}$) |
|---|---|---|---|---|
| PA$c_{551}$[a] | 80.23 ± 5.86 | 0.22 ± 0.02 | 86.4 ± 0.7 | −5.42 ± 0.5 |
| PH$c_{552}$ | 84.49 ± 12.9 | 0.22 ± 0.04 | 108.0 ± 0.4 | 0 |
| HT$c_{552}$[a] | 121.4 ± 4.83 | 0.31 ± 0.01 | 121.1 ± 1.0 | 4.01 ± 0.3 |

[a] Data are from Oikawa et al, and each parameter has been calculated here as described below (*13*). The temperature of the midpoint of the thermal unfolding ($T_m$) and the unfolding enthalpy change at $T_m$, $\Delta H(T_m)$, were calculated from curve fitting of the resulting CD values versus the temperature data on the basis of the van't Hoff analysis. The unfolding entropy change at $T_m$, $\Delta S(T_m)$ was calculated using the equation $\Delta S(T_m) = \Delta H(T_m)/T_m$. The free-energy change, $\Delta G$, at $T_m$ of PH$c_{552}$, where $\Delta G$ of PH$c_{552}$ is equal to zero, was calculated using the equation $\Delta G = \Delta H(T_m) + \Delta C_p(T - T_m) - T[\Delta H(T_m)/T_m - \Delta C_p \ln(T/T_m)]$. Here, change in the heat capacity, $\Delta C_P$, of PA$c_{551}$ and HT$c_{552}$ in oxidized conditions at pH 3.6 (*13*) was employed.

Table 3: Thermodynamic Parameters Obtained from Chemical Denaturation

| | $C_m$ (M) | $m$ (kcal mol$^{-1}$ M$^{-1}$) | $\Delta G_{H2O}$ (kcal mol$^{-1}$) | $\Delta\Delta G_{H2O}$(PH$c_{552}$) (kcal mol$^{-1}$) |
|---|---|---|---|---|
| PA$c_{551}$[a] | 2.06 ± 0.01 | 2.72 ± 0.27 | 5.61 ± 0.58 | −2.13 ± 0.6 |
| PH$c_{552}$ | 2.97 ± 0.05 | 2.61 ± 0.43 | 7.74 ± 1.31 | 0 |
| HT$c_{552}$[b] | 4.46 ± 0.18 | 2.40 ± 0.52 | 10.73 ± 2.47 | 2.99 ± 1.2 |

[a] Unpublished results (Sambongi, Y.). [b] Data are from Oikawa et al (*13*). The free-energy change in $H_2O$ ($\Delta G_{H2O}$) and the dependence of $\Delta G$ on the Gdn-HCl concentration ($m$) were determined by a least-squares fit of the data from the transition region using the equation $\Delta G = \Delta G_{H2O} - m$[Gdn-HCl]. The midpoint of the Gdn-HCl denaturation ($C_m$) was the concentration of Gdn-HCl at which the $\Delta G$ value became zero. $\Delta\Delta G_{H2O}$(PH$c_{552}$) was the difference of $\Delta G_{H2O}$ calculated from the value of PH$c_{552}$ as reference. These chemical denaturation experiments were performed at 25 °C.

which was in the intermediate melting temperature range between 86.4 °C of PA$c_{551}$ and 121.1 °C of HT$c_{552}$ (*13*). Furthermore, the intermediate thermal stability is obvious in the fact that the free-energy change $\Delta G$ values at the transition temperature of PH$c_{552}$ were −5.42 kcal mol$^{-1}$ for PA$c_{551}$ and 4.01 kcal mol$^{-1}$ for HT$c_{552}$.

The chemical denaturation experiments, which were performed at 25 °C with Gdn-HCl, also showed a moderate stability of PH$c_{552}$ (Table 3); PH$c_{552}$ exhibited the $C_m$ value of 2.97 M, while the $C_m$ values for PA$c_{551}$ and HT$c_{552}$ are 2.06 and 4.46 M (*13*), respectively. The differences in free-energy change at the finite dilution for the chemical denaturation from that of PH$c_{552}$, $\Delta\Delta G_{H2O}$, were −2.13 kcal mol$^{-1}$ for PA$c_{551}$ and 2.99 kcal mol$^{-1}$ for HT$c_{552}$. These results from thermal and chemical denaturation revealed that PH$c_{552}$ has an intermediate stability compared with HT$c_{552}$ and PA$c_{551}$. The order of stability among the three cytochromes *c* reflects the optimal growth temperature of the original bacteria.

*Sequence Comparison among PAc$_{551}$, PHc$_{552}$, and HTc$_{552}$.* The cloned sequence showed that PH$c_{552}$ shares sequence identities of 50.6% with PA$c_{551}$ and 54.4% with HT$c_{552}$. Alignments of these three cytochromes are shown in Figure 2. The identity among PA$c_{551}$, PH$c_{552}$, and HT$c_{552}$ was 40%, while there were the following three major differences: (i) the deletion of two amino acid residues, ED, at the N-terminus (PH$c_{552}$ and HT$c_{552}$); (ii) the deletion of GQ (PA$c_{551}$) or GR (HT$c_{552}$) in PH$c_{552}$; and (iii) the insertion of a proline residue in PH$c_{552}$ at the location between Asn64 and Ala65 of PA$c_{551}$.

Corresponding to the five residues that are responsible for the different thermal stability between PA$c_{551}$ and HT$c_{552}$, PH$c_{552}$ has Ala5[7], Met11[13], Tyr32[34], Lys39[43], and Val75[78]. The numbers in the square brackets represent the residue numbers in the sequence of PA$c_{551}$, which make it easy to grasp the counterparts in PA$c_{551}$. Among them, Ala5-[7], Met11[13], and Tyr32[34] are the same as those in HT$c_{552}$, respectively, while Val75[78] is the same as in PA$c_{551}$. Lys39[43] is different from Glu43 in PA$c_{551}$ and from Tyr41[43] in HT$c_{552}$. It is quite natural to expect that the three amino acid residues coinciding with those of HT$c_{552}$ contribute to the enhanced stability of PH$c_{552}$ and the one coinciding with PA$c_{551}$ to decrease its stability.

*Overall Structure of PHc$_{552}$.* In the crystal structure analysis of PH$c_{552}$, the phase of the molecular replacement method using PA$c_{551}$ (PDB code: 351C) as the model provided a clean map and well-defined connectivity in the deletion and insertion loops. The final refined model of the PH$c_{552}$ included 31 water molecules, and the crystallographic *R*-factor ($R_{free}$) was 18.1% (21.8%). The coordinate error based on the statistics of Luzzati (*37*) was estimated as 0.215 Å. The crystal structure of PH$c_{552}$ exhibits a typical class I *c*-type cytochrome fold embedding the heme prosthetic group by thioether covalent bonds with Cys10[12] and Cys13[15]. The protein chain has four α-helices, αA (residues 2−7), αB (residues 25−31), αC (residues 37−46), and αD (residues 65−75), and two $3_{10}$ helices, $3_{10}$A (residues 10−12) and $3_{10}$B (residues 34−36). In PA$c_{551}$ and HT$c_{552}$, residues from 34 to 39 formed two consecutive turns. There

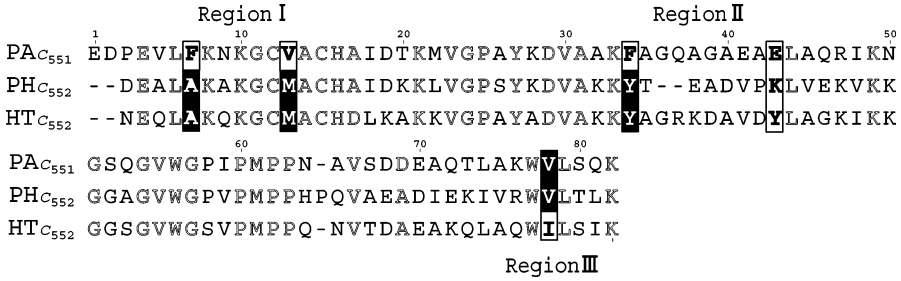


FIGURE 2: Multiple sequence alignment of PA$c_{551}$, PH$c_{552}$, and HT$c_{552}$. The identical residues in PA$c_{551}$, PH$c_{552}$, and HT$c_{552}$ are written in outline letters. Gaps in the alignment are indicated by a dash. The five residues responsible for the stability in HT$c_{552}$ are surrounded by boxes, and the same residues in PA$c_{551}$, PH$c_{552}$, and HT$c_{552}$ are highlighted in black.

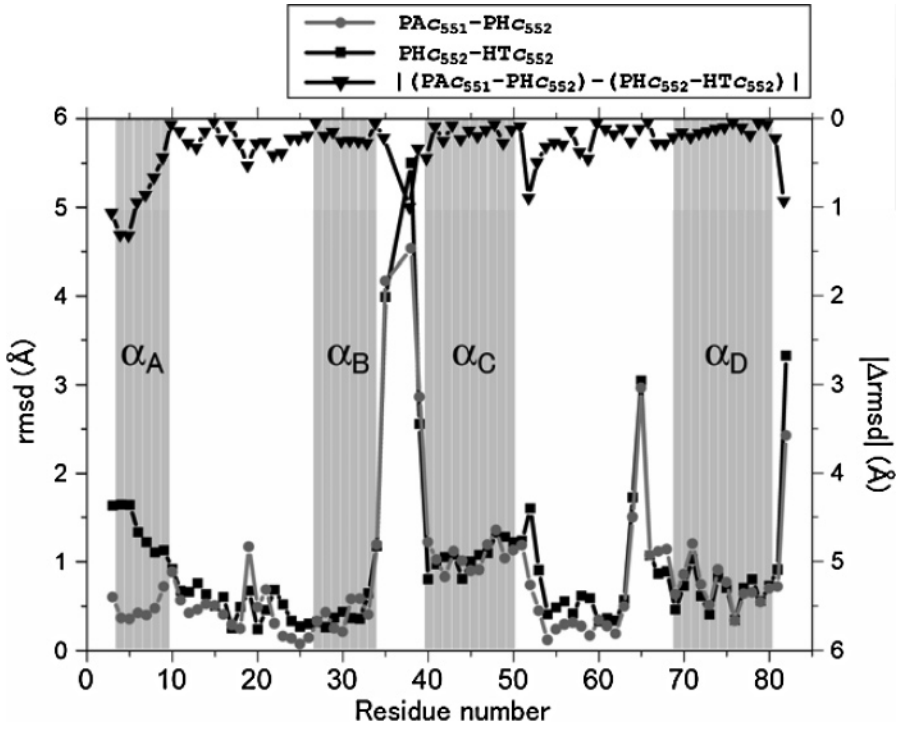


FIGURE 3: The rmsd values plotted against the residue number of PA$c_{551}$. Plots are shown for PA$c_{551}$−PH$c_{552}$ (gray, closed circles), PH$c_{552}$−HT$c_{552}$ (black, closed square), and the absolute value of the difference between PA$c_{551}$−PH$c_{552}$ and PH$c_{552}$−HT$c_{552}$ (black, inverted triangle). The right-hand axis (on a scale of 0−6) refers to |Δrmsd|. Four helices of PA$c_{551}$ are shown on gray background.

was the deletion of two residues in this region of PH$c_{552}$. A $3_{10}$ helix was formed as a result, and the loop region was stabilized.

*Structural Comparison among PAc551, PHc552, and HTc552.* The backbone structure of PH$c_{552}$ was compared with those of PA$c_{551}$ (PDB code, 351C) and HT$c_{552}$ (PDB code, 1YNR). The average backbone rmsd values were 1.28 Å for PA$c_{551}$−PH$c_{552}$, 0.80 Å for PA$c_{551}$−HT$c_{552}$, and 1.13 Å for PH$c_{552}$−HT$c_{552}$. The rmsd values of PA$c_{551}$−PH$c_{552}$ and PH$c_{552}$−HT$c_{552}$ and the differences in the rmsd values between PA$c_{551}$−PH$c_{552}$ and PH$c_{552}$−HT$c_{552}$ (|Δrmsd|) were plotted against the residue number of PA$c_{551}$ in Figure 3. Large |Δrmsd| values that exceeded 1.0 Å were found in the region from the third to fifth residues, which was located at αA helix. Thus, these three structures had the difference only at αA, and indicated very similar folds.

In our previous paper, three regions of the molecular surface, where the five key residues contributing to the thermal stability are localized on the surface, were noted and named as regions I, II, and III (*15*).

*Region I, F7A/V13M.* Among the five residues, two residues, Phe7 and Val13, and Ala5[7] and Met11[13], are located in region I of PA$c_{551}$ and HT$c_{552}$, respectively. As mentioned before, both residues in PH$c_{552}$ are the same as those in HT$c_{552}$. In PH$c_{552}$, Ala5[7] and Met11[13] were also spatially arranged in this region. As shown in Figure 4a, the side chain of Phe7 in PA$c_{551}$ occupied a rather large space inside the molecule so that the side chain of Val13 protruded into the solvent. On the other hand, in PH$c_{552}$ and HT$c_{552}$, Met11[13] could enter into the space, because the bulky side chain of Phe7 was substituted by the small methyl group of Ala5[7] to make room. Consequently, the tight van der Waals interactions of the side chains of Ala and Met inside the molecule led to the formation of a hydrophobic core to provide the enhanced thermal stabilities for PH$c_{552}$ and HT$c_{552}$.

Additionally, there were apparent differences around region I among the three molecules, as shown in Figure 4b, that orients αA outside toward the solvent in PA$c_{551}$ compared to those of PH$c_{552}$ and HT$c_{552}$. Each angle between the αAs was 16.4° for PA$c_{551}$−PH$c_{552}$ and 0.7° for PH$c_{552}$−HT$c_{552}$. Phe7 seems to prop the αA to be pushed out in PA$c_{551}$. However, it should be considered whether these differences were caused by the flexibility of αA in the

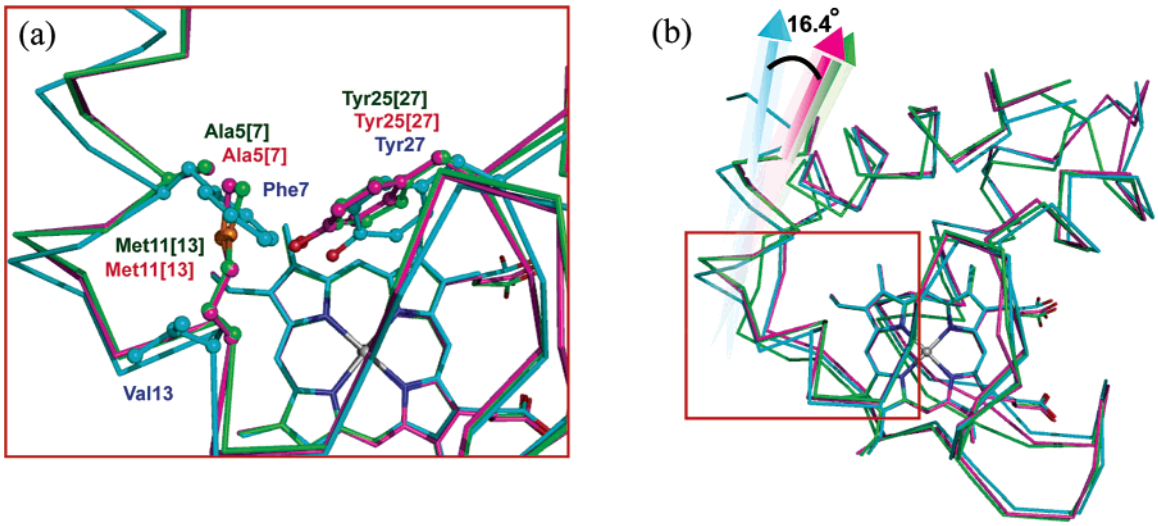


FIGURE 4: (a) Zoom-in of the red box in panel b. Two residues out of the five residues of interest, Phe7 and Val13, Ala5[7] and Met11[13], and Ala5[7] and Met11[13] in region I of PA$c_{551}$, PH$c_{552}$, and HT$c_{552}$, respectively, are shown as stick-and-ball model. Tyr27, which forms the hydrogen bond with Met11[13] (SD), is also shown. (b) Structural alignment of PA$c_{551}$, PH$c_{552}$, and HT$c_{552}$ backbone structures. The color code used for the structural illustrations is as follows: cyan for PA$c_{551}$, green for PH$c_{552}$, and magenta for HT$c_{552}$. The arrows indicate axis of αA. The helix−helix angle between αA of PA$c_{551}$ and PH$c_{552}$ was 16.4°.

vicinity of the N-terminal regions of the proteins. At the N-termini of these three structures, the hydrogen bond between the side chain of Asp2 for PA$c_{551}$ (or the first residue for PH$c_{552}$ and HT$c_{552}$) and the main chain of Leu6 (Leu4-[6] for PH$c_{552}$ and HT$c_{552}$) was found to form the N-cap motif (*38*). Indeed, the average *B*-value of the first four residues at the N-terminal of PH$c_{552}$ was 20.1 Å$^2$, which was smaller than that of the last four residues at the C-terminal region (32.4 Å$^2$) in which these four residues had no specific interaction with other groups. Hence, the differences of the αA orientation were not due to the flexibility of the N-terminal chain but the packing change induced by the mutations of Phe7 to Ala5[7] and Val13 to Met11[13]. It is probable that the rather compact structures of PH$c_{552}$ and HT$c_{552}$ enhance the stabilities of these molecules by increasing van der Waals interactions.

Regarding HT$c_{552}$, Travaglini-Allocatelli et al. suggested the hydrogen bond formation between Met11[13] (SD) and Tyr25[27] (OH) is based on the fact that these two groups are adjacent to each other with the distance of 3.19 Å (*17*). Such a hydrogen bond, especially in the hydrophobic environment, should contribute largely to stabilizing the conformation of HT$c_{552}$. The corresponding distance between Met11[13] and Tyr25[27] in PH$c_{552}$ was 3.54 Å, which is too long to form a hydrogen bond. Thus, this additional hydrogen bond in HT$c_{552}$ possibly contributes to the largest enhanced stability.

*Region II, F34Y/E43Y*. In region II, two residues, Phe34 and Glu43, and Tyr32[34] and Tyr41[43], are located for PA$c_{551}$ and HT$c_{552}$, respectively. In these positions of PH$c_{552}$, Tyr32[34] was the same amino acid as that of HT$c_{552}$, while Lys39[43] corresponds to neither Glu43 of PA$c_{551}$ nor Tyr41-[43] of HT$c_{552}$. As shown in Figure 5, the hydroxyl group of Tyr32[34] of PH$c_{552}$ formed a bifurcated hydrogen bond with the NZ atom of Lys31[33] and carboxyl group (O1A) on propionic acid of the heme. Additionally, a hydrogen bond network, Lys31[33] (NZ)−Tyr32[34] (OH)−heme (O1A)−heme (O2A)−Lys43[47] (NZ)−heme (O2D) was made up to build a bridge between αB and αC. In the case of PA$c_{551}$, Phe34 does not have a hydroxyl group and each propionic acid of the heme independently interacted with Arg47 (NH2) and Ser52 (OH). Thus, the hydrogen bond network, which was found in PH$c_{552}$, did not exist in PA$c_{551}$. HT$c_{552}$ has a hydrogen bond network, Lys31[33] (NZ)−Tyr32[34] (OH)−heme (O1A)−heme (O2A)−Lys45[47] (NZ) like that of PH$c_{552}$. Furthermore, the additional hydrogen bond was formed between Tyr41[43] (OH) and heme (O1A) as Travaglini-Allocatelli et al. described (*17*). On the other hand, Lys39[43] of PH$c_{552}$ did not participate in the hydrogen bond network because the distance between Lys39[43] (NZ) and Asp36[40] (OD) was 3.22 Å in PH$c_{552}$, which allowed them to form an attractive electrostatic interaction. As described above, these interactions connecting αB and αC were formed in PH$c_{552}$ and HT$c_{552}$ but not in PA$c_{551}$. HT$c_{552}$ had an additional residue (Tyr41[43]) involving this interaction compared to PA$c_{551}$. Therefore, it seems reasonable to conclude that these residues in region II significantly contribute to determine the order of stability of the molecules by the improvement of the electrostatic interactions with the heme in the center of cytochrome *c* fold.

However, in the crystal of HT$c_{552}$, there were four molecules in the asymmetric unit, and the crystallization reagents were found in the molecular interfaces (*17*). There were eight 2-methyl-2,4-pentandiol (MPD) molecules and three sulfate ions. It is possible that some artifacts were caused by these contaminations. For example, MPD found around Tyr41[43] of each molecular surface in the asymmetric unit might affect the orientation of Tyr41[43] to force its side chain to form a hydrogen bond with the propionate group of the heme. We will discuss this possibility later in relation to the solution structure of HT$c_{552}$ determined by NMR.

*Region III, V78I*. In region III, among the five residues of interest, Val78 in PA$c_{551}$ is substituted by Ile76[78] in HT$c_{552}$, while PH$c_{552}$ retains Val75[78]. As shown in Figure 6, there is a hydrophobic core consisting of the heme and αD in this region. The hydrophobic side chains of these three residues at the 78th positions protrude toward the heme with almost

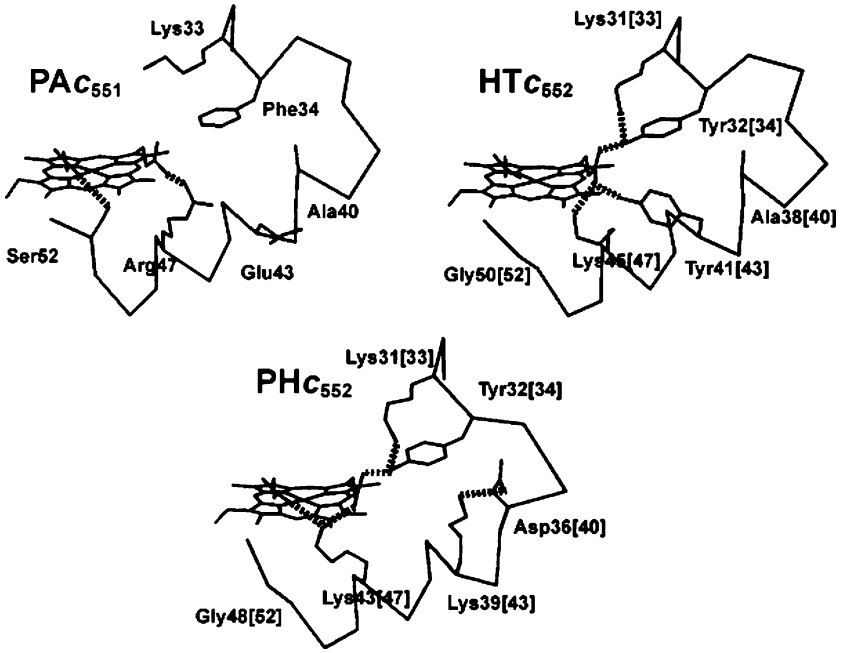


FIGURE 5: The hydrogen bond networks in region II of PA$c_{551}$, PH$c_{552}$, and HT$c_{552}$. Backbone structures from 31 to 53 and the counterparts of 33, 34, 40, 43, 47, and 52 in PA$c_{551}$ are shown. Dashed lines indicate the electrostatic interactions.

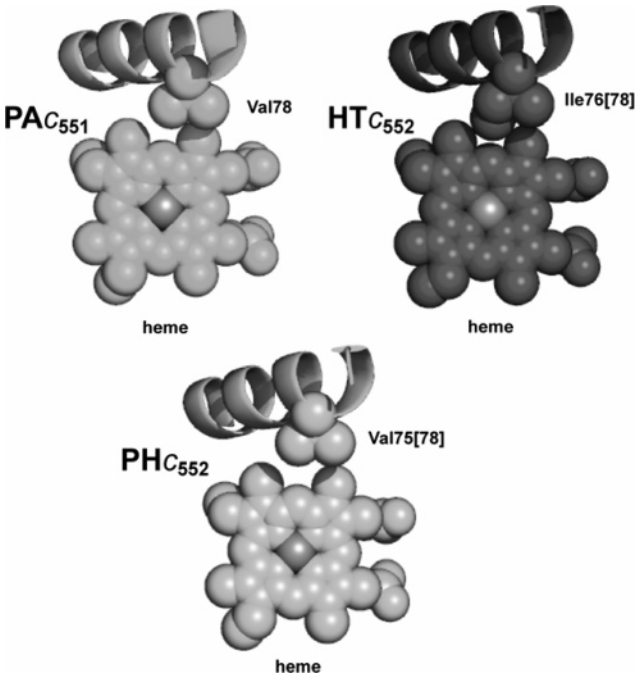


FIGURE 6: The hydrophobic core in region III. Heme and Val78, Val75[78], and Ile 76[78] are shown in space-filling model. αD is displayed as a ribbon model.

the same $\chi_1$ angles. There is a gap between the heme and Val78 in PA$c_{551}$ and PH$c_{552}$ compared to that in HT$c_{552}$. This gap was filled by the methyl group of Ile76[78] (CD1) in the case of HT$c_{552}$. This difference in packing density should reflect on the intensity of hydrophobic interaction. Thus, the variation from Val to Ile provides higher stability for HT$c_{552}$ than PA$c_{551}$ and PH$c_{552}$.

*Recalculated Solution Structure of HTc*$_{552}$. To compare the structures in crystal and solution, we refined the solution structure of HT$c_{552}$ by using distributed computational implementation. The refined structure showed the significant improvement for the structural quality (a residue-averaged rmsd for 20 structures ensemble is 0.34 ± 0.05 Å) (Figure 7a). The solution structure is very similar to the crystal structure of HT$c_{552}$ with an overall average rmsd of 0.9 Å.

In the crystal of HT$c_{552}$, there was the possibility that some artifacts were caused by MPD molecules as described above (*17*). This was clearly shown to be unlikely by the fact that, in the recalculated solution structure, the side chain of Tyr41-[43] was oriented in the direction to the propionate group and located within the hydrogen bond forming distance to the heme in solution as well (Figure 7b).

The solution structure's rmsd values of the atomic coordinates for each residue among 20 structures ensemble were plotted against the number of amino acid residues of the HT$c_{552}$ molecule with *B*-values in its crystal structure determined by Travaglini-Allocatelli et al. (*17*) in Figure 8. It is noteworthy that the tendency of the rmsd is quite similar to that of *B*-values. The resemblance for the uncertainty of atomic coordinates indicates that the local flexibilities of the protein molecule in solution are retained in the crystal. This strongly supports the hypothesis that we could assume the crystal structures discussed above should reflect the properties of the molecule in solution.

## CONCLUSION

Here, it has been clearly demonstrated by CD measurements that PH$c_{552}$ has a stability which is between those of PA$c_{551}$ and HT$c_{552}$ as expected from the growth temperature of its source; *H. thermoluteolus* (*P. hydrogenoermophila*). Furthermore, we determined the structure of PH$c_{552}$ by X-ray analysis with a resolution of 2.2 Å. The result showed that its main-chain folding is similar to those of PA$c_{551}$ and HT$c_{552}$. Thus, we concluded that the thermal stabilities of these cytochromes *c* are controlled by the side-chain contributions. Our comparative studies on PA$c_{551}$ and HT$c_{552}$, employing mutational experiments combined with extensive structural analyses, had identified five residues located in the three regions that control the overall conformational stabilities of the molecules.

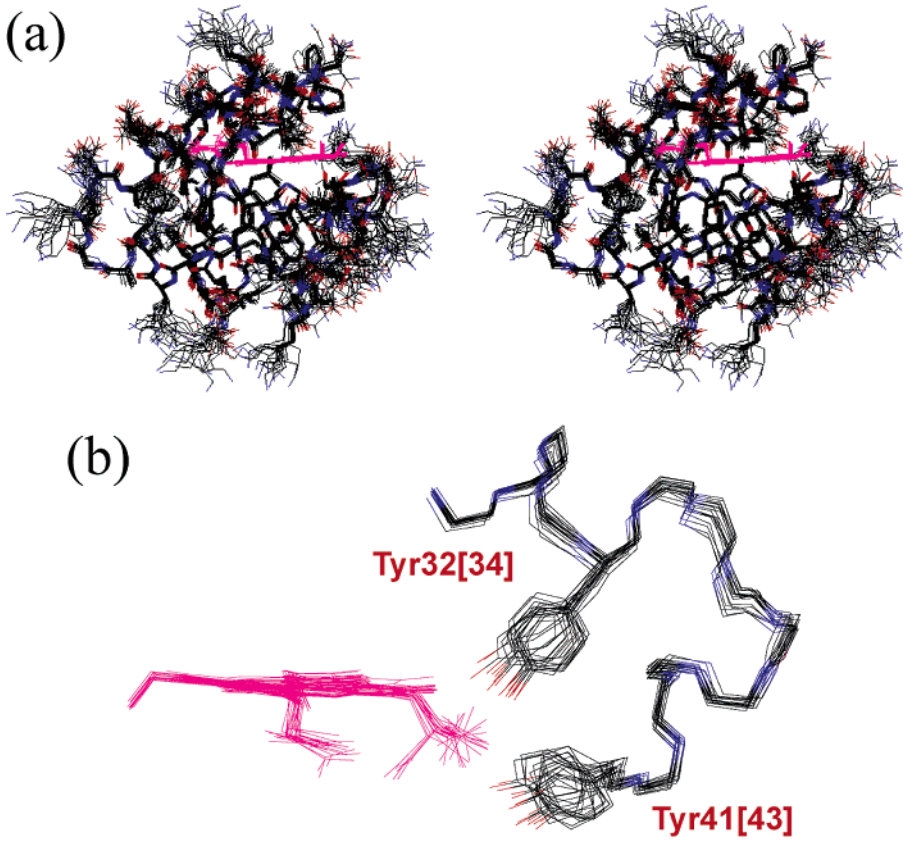


FIGURE 7: (a) The solution−structure ensemble (stereoview) of recalculated HT$c_{552}$ using NMR constraints (*11*) and distributed computing technique. The heme is indicated in magenta. (b) The hydrogen bond network formed by Tyr32[34], Tyr41[43], and heme in the solution structure. The backbone structure from Val28[30] to Tyr41[43] and the side chains of Tyr32[34] and Tyr41[43] in HT$c_{552}$ are shown.

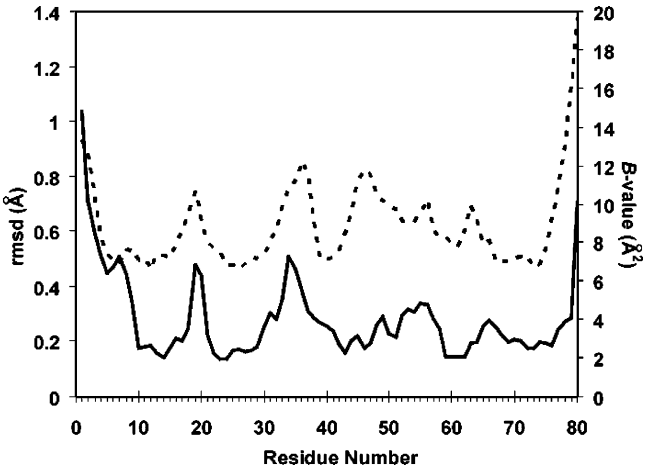


FIGURE 8: The rmsd values (full line, left axis) and *B*-values of the crystal structure (dashed line, right axis) (PDB code, 1YNR) plotted against residue number.

Expanding this comparative study by incorporating PH$c_{552}$, we tried to obtain a deeper insight into the mechanism by which these five residues control stability. The results revealed that they provide the stability with, in region I, improved van der Waals interactions by packing optimization at αA; in region II, attractive electrostatic interactions with the heme propionate group; and in region III, favorable van der Waals interaction with the heme. These local interactions contribute independently to the overall stability, so that the stabilization by these interactions seems to act in an additive manner.

Here, we have demonstrated that just a small number of amino acid residues determine the overall molecular stability. It is especially interesting that, in naturally occurring proteins, the additivities of these effects are utilized to obtain their characteristic stabilities to survive in the wide range of thermal conditions.

## ACKNOWLEDGMENT

We gratefully acknowledge Dr. E. R. Stimson for reading the manuscript and for useful comments. T. Sonoyama is thanked for stimulating discussions and for exchanging information.

## SUPPORTING INFORMATION AVAILABLE

Figure showing the reversibility of PH$c_{552}$. This material is available free of charge via the Internet at http://pubs.acs.org.

## REFERENCES

1. Jaenicke, R., and Böhm, G. (1998) The stability of proteins in extreme environments, *Curr. Opin. Struct. Biol. 8*, 738−748.
2. Jaenicke, R. (2000) Stability and stabilization of globular proteins in solution, *J. Biotechnol. 79*, 193−203.
3. Singer, G. A., and Hickey, D. A. (2003) Thermophilic prokaryotes have characteristic patterns of codon usage, amino acid composition and nucleotide content, *Gene 317*, 39−47.
4. Orengo, C. A., and Thornton, J. M. (2005) Protein families and their evolution−a structural perspective, *Annu. Rev. Biochem. 74*, 867−900.
5. Bordo, D., and Bork, P. (2002) The rhodanese/Cdc25 phosphatase superfamily. Sequence−structure function relations, *EMBO Rep. 3*, 741−746.

6. Sambongi, Y., Uchiyama, S., Kobayashi, Y., Igarashi, Y., and Hasegawa, J. (2002) Cytochrome *c* from a thermophilic bacterium has provided insights into the mechanisms of protein maturation, folding, and stability, *Eur. J. Biochem. 269*, 3355−3361.
7. Kimura, S., Nakamura, H., Hashimoto, T., Oobatake, M., and Kanaya, S. (1992) Stabilization of *Escherichia coli* ribonuclease HI by strategic replacement of amino acid residues with those from the thermophilic counterpart, *J. Biol. Chem. 267*, 21535−21542.
8. Haney, P. J., Stees, M., and Konisky, J. (1999) Analysis of thermal stabilizing interactions in mesophilic and thermophilic adenylate kinases from the genus *Methanococcus*, *J. Biol. Chem. 274*, 28453−28458.
9. Criswell, A. R., Bae, E., Stec, B., Konisky, J., and Phillips, G. N., Jr. (2003) Structures of thermophilic and mesophilic adenylate kinases from the genus *Methanococcus*, *J. Mol. Biol. 330*, 1087−1099.
10. Bae, E., and Phillips, G. N., Jr. (2004) Structures and analysis of highly homologous psychrophilic, mesophilic, and thermophilic adenylate kinases, *J. Biol. Chem. 279*, 28202−28208.
11. Hasegawa, J., Yoshida, T., Yamazaki, T., Sambongi, Y., Yu, Y., Igarashi, Y., Kodama, T., Yamazaki, K., Kyogoku, Y., and Kobayashi, Y. (1998) Solution structure of thermostable cytochrome *c*-552 from *Hydrogenobacter thermophilus* determined by $^1$H-NMR spectroscopy, *Biochemistry 37*, 9641−9649.
12. Hasegawa, J., Shimahara, H., Mizutani, M., Uchiyama, S., Arai, H., Ishii, M., Kobayashi, Y., Ferguson, S. J., Sambongi, Y., and Igarashi, Y. (1999) Stabilization of *Pseudomonas aeruginosa* cytochrome $c_{551}$ by systematic amino acid substitutions based on the structure of thermophilic *Hydrogenobacter thermophilus* cytochrome $c_{552}$, *J. Biol. Chem. 274*, 37533−37537.
13. Oikawa, K., Nakamura, S., Sonoyama, T., Ohshima, A., Kobayashi, Y., Takayama, S. J., Yamamoto, Y., Uchiyama, S., Hasegawa, J., and Sambongi, Y. (2005) Five amino acid residues responsible for the high stability of *Hydrogenobacter thermophilus* cytochrome $c_{552}$: reciprocal mutation analysis, *J. Biol. Chem. 280*, 5527−5532.
14. Hasegawa, J., Uchiyama, S., Tanimoto, Y., Mizutani, M., Kobayashi, Y., Sambongi, Y., and Igarashi, Y. (2000) Selected mutations in a mesophilic cytochrome *c* confer the stability of a thermophilic counterpart, *J. Biol. Chem. 275*, 37824−37828.
15. Uchiyama, S., Hasegawa, J., Tanimoto, Y., Moriguchi, H., Mizutani, M., Igarashi, Y., Sambongi, Y., and Kobayashi, Y. (2002) Thermodynamic characterization of variants of mesophilic cytochrome *c* and its thermophilic counterpart, *Protein Eng. 15*, 455−462.
16. Ichiki, S., Nakamura, S., Ohkubo, T., Kobayashi, Y., Hasegawa, J., Uchiyama, S., Nishihara, H., Mizuta, K., and Sambongi, Y. (2005) Cloning, expression, crystallization and preliminary X-ray characterization of cytochrome $c_{552}$ from a moderate thermophilic bacterium, *Hydrogenophilus thermoluteolus*, *Acta Crystallogr. F61*, 395−398.
17. Travaglini-Allocatelli, C., Gianni, S., Dubey, V. K., Borgia, A., Di Matteo, A., Bonivento, D., Cutruzzola, F., Bren, K. L., and Brunori, M. (2005) An obligatory intermediate in the folding pathway of cytochrome $c_{552}$ from *Hydrogenobacter thermophilus*, *J. Biol. Chem. 280*, 25729−25734.
18. Takashima, H., Mimura, N., Ohkubo, T., Yoshida, T., Tamaoki, H., and Kobayashi, Y. (2004) Distributed computing and NMR constraint-based high-resolution structure determination: applied for bioactive peptide endothelin-1 to determine C-terminal folding, *J. Am. Chem. Soc. 126*, 4504−4505.
19. Takashima, H., Tamaoki, H., Teno, N., Nishi, Y., Uchiyama, S., Fukui, K., and Kobayashi, Y. (2004) Hydrophobic core around tyrosine for human endothelin-1 investigated by photochemically induced dynamic nuclear polarization nuclear magnetic resonance and matrix-assisted laser desorption ionization time-of-flight mass spectrometry, *Biochemistry 43*, 13932−13936.
20. Takashima, H., Yoshida, T., Ishino, T., Hasuda, K., Ohkubo, T., and Kobayashi, Y. (2005) Solution NMR structure investigation for releasing mechanism of neocarzinostatin chromophore from the holoprotein, *J. Biol. Chem. 280*, 11340−11346.
21. Zhang, Y., Arai, H., Sambongi, Y., Igarashi, Y., and Kodama, T. (1998) Heterologous expression of *Hydrogenobacter thermophilus* cytochrome *c*-552 in the periplasm of *Pseudomonas aeruginosa*, *J. Ferment. Bioeng. 85*, 346−349.
22. Ohshima, A., Uchiyama, S., Nakano, H., Yoshida, T., Ohkubo, T., and Kobayashi, Y. (2003) CD measurement of aqueous protein solution at high temperature up to 180°C—Thermodynamic analysis of thermophilic protein by pressure-proof cell compartment, *Lett. Pept. Sci. 10*, 539−543.
23. Uchiyama, S., Ohshima, A., Nakamura, S., Hasegawa, J., Terui, N., Takayama, S. J., Yamamoto, Y., Sambongi, Y., and Kobayashi, Y. (2004) Complete thermal-unfolding profiles of oxidized and reduced cytochromes *c*, *J. Am. Chem. Soc. 126*, 14684−14685.
24. Marky, L. A., and Breslauer, K. J. (1987) Calculating thermodynamic data for transitions of any molecularity from equilibrium melting curves, *Biopolymers 26*, 1601−1620.
25. Santoro, M. M., and Bolen, D. W. (1988) Unfolding free energy changes determined by the linear extrapolation method. 1. Unfolding of phenylmethanesulfonyl α-chymotrypsin using different denaturants, *Biochemistry 27*, 8063−8068.
26. Pflugrath, J. W. (1999) The finer things in X-ray diffraction data collection, *Acta Crystallogr. D55*, 1718−1725.
27. Vagin, A., and Teplyakov, A. (1997) MOLREP: An automated program for molecular replacement, *Acta Crystallogr. D30*, 1022−1025.
28. Brunger, A. T., Adams, P. D., Clore, G. M., DeLano, W. L., Gros, P., Grosse-Kunstleve, R. W., Jiang, J. S., Kuszewski, J., Nilges, M., Pannu, N. S., Read, R. J., Rice, L. M., Simonson, T., and Warren, G. L. (1998) Crystallography & NMR system: A new software suite for macromolecular structure determination, *Acta Crystallogr. D54*, 905−921.
29. Murshudov, G. N., Vagin, A. A., Lebedev, A., Wilson, K. S., and Dodson, E. J. (1999) Efficient anisotropic refinement of macromolecular structures using FFT, *Acta Crystallogr. D55*, 247−255.
30. McRee, D. E. (1999) XtalView/Xfit—A versatile program for manipulating atomic coordinates and electron density, *J. Struct. Biol. 125*, 156−165.
31. Laskowski, R. A., MacArthur, M. W., Moss, D. S., and Thornton, J. M. (1993) PROCHECK: A program to check the stereochemical quality of protein structures, *J. Appl. Crystallogr. 26*, 283−291.
32. Kabsch, W., and Sander, C. (1983) Dictionary of protein secondary structure: Pattern recognition of hydrogen-bonded and geometrical features, *Biopolymers 22*, 2577−2637.
33. Martin, A. C. R. (1996) ProFit, http://www.bioinf.org.uk/software/profit/.
34. DeLano, W. L. (2002) The PyMOL molecular graphics system, http://pymol.sourceforge.net.
35. Koradi, R., Billeter, M., and Wüthrich, K. (1996) MOLMOL: A program for display and analysis of macromolecular structures, *J. Mol. Graphics 14*, 51−55.
36. Schwieters, C. D., Kuszewski, J. J., Tjandra, N., and Clore, G. M. (2003) The Xplor-NIH NMR molecular structure determination package, *J. Magn. Reson. 160*, 65−73.
37. Luzzati, V. (1952) Traitement statistique des erreurs dans la determination des structures cristallines. *Acta Crystallogr. 5*, 802−810.
38. Richardson, J. S., and Richardson, D. C. (1988) Amino acid preferences for specific locations at the ends of alpha helices, *Science 240*, 1648−1652.


BI0520131